Fluorinated biphenyl aromatic polyimides for gas separation applications. Real gas mixture study.

Sandra Rico-Martínez[1], Mario Rojas-Rodriguez[2], Noelia Esteban[1], Laura Matesanz-Niño[3,4], Marta Juan y Seva[3], Larissa Alexandrova[2], Benny D. Freeman[5], Cristina Álvarez[3,4*], Ángel E. Lozano[1,3,4,*], Carla Aguilar-Lugo[2,*],

[1]IU CINQUIMA, University of Valladolid, Paseo Belén 5, E-47011 Valladolid, Spain.

[2]Instituto de Investigaciones en Materiales, Universidad Nacional Autónoma de México, Circuito Exterior s/n, Ciudad Universitaria, 04510 México City, Mexico.

[3]Institute of Polymer Science and Technology, ICTP-CSIC, Juan de la Cierva 3, E- 28006 Madrid, Spain.

[4]SMAP, UA-UVA_CSIC, Associated Research Unit to CSIC. University of Valladolid, School of Sciences, Paseo Belén 7, E-47011 Valladolid, Spain.

[5]McKetta Department of Chemical Engineering, Texas Materials Institute, The University of Texas at Austin, 200 E Dean Keeton St., Austin, TX 78712-1589

*Corresponding authors: Carla Aguilar-Lugo; carla.aguilar@iim.unam.mx, Cristina Álvarez; E-mail: cristina.alvarez@ictp.csic.es, and Ángel E. Lozano; E-mail: lozano@ictp.csic.es

Abstract. Three aromatic polyimides (PIs) based on diamines containing biphenyl unit and CF_3-groups in *m*-position to amines and 6FDA of high molecular weights were synthesized. The polymers differed by number of methyl-substituents in biphenyl moiety, as 6FDA-BFAPB, PI without methyl substituents, 6FDA-4MeBFAPB, PI with 4 methyl groups, and 6FDA-4MeBFAPB, PI with 6 methyl groups. The comparative analysis of the polymers' properties was performed with focus on their gas transport properties. All PIs demonstrated high thermostability, with decomposition temperature above 450 ºC in inert atmosphere and char yield of 45-50 % but were readily soluble at room temperature even in common organic solvents. The Tg's of PI bearing methyl groups were notably higher than that of 6FDA-BFAPB, indicating their more rigid backbone chains. Detailed investigation of the PIs' gas transport properties was also made for pure gases and real gas mixture in the wide interval of pressures. It was shown that introduction of the methyl substituents in the main polymer chain resulted in an important improvement of the gas transport properties; both methylated PIs were located much closer to the Robeson limit.

1. Introduction

Nowadays, polymeric materials such as membranes have become a profitable way to separate acid gases and impurities from natural gas since they offer benefits compared to other separation technologies, such as being an ecological attractive, easy to operate, and reducing costs in comparison with conventional industrial processes[1–4]. However, commercially available membranes, polysulfones, cellulose acetate, and polyaramids, exhibit limited permeability and selectivity properties, reducing their large scale use[5,6].

Among various classes of polymers studied for gas separation, aromatic polyimides are considered as potential candidates due to an optimal combination of their properties, excellent thermal, chemical, and mechanical resistance, as well as an easiness of membranes' formation thanks to their solubility in various organic solvents. However, well-known trade-off between permeability and selectivity polyimides application[6–9]. Since these parameters are related to the membrane productivity (permeability) and efficiency (selectivity) of the separation process, the search for the ideal polymeric membrane remains a challenge.

Polymers with high free volume and rigidity are required for gas separation membranes in order to increase the selectivity and permeability simultaneously[10–14]. For this, bulky groups such as methyl, *tert*-butyl, trifluoromethyl, silanes, are commonly introduced into the main chain; decreasing the packing between chains, increasing the fractional free volume and the permeability [15–19]; Additionally, such modification reduces the segmental mobility, facilitates behavior as molecular sieves, and, hence, promotes high selectivity [20,21].

This article reports the synthesis of custom-designed monomers (diamines) which give polyimides with improved gas separation performance. [14,22–24] Our strategy was focused on increasing significantly the rigidity of the macromolecular chains introducing biphenyl and methyl-substituted biphenyl units into the diamine structures. Besides, the presence of bulky CF_3-group in *ortho*-position to the ether link restricts the rotation around this bond, that should additionally improve the permeability without important reduction in the selectivity (see **Figure 1** for the diamines' structures). Thus, three diamines were synthesized, and the polyimides based on them and 6FDA dianhydride were obtained and characterized. The of the polymers' synthesis is shown in **Figure2**.

6FDA was selected because the membranes derived from this dianhydride demonstrated good transport properties together with the substantial improvement in the processability due to the presence of bulky hexafluoropropylidene, -$C(CF_3)_3$-, unit[7,18,25].

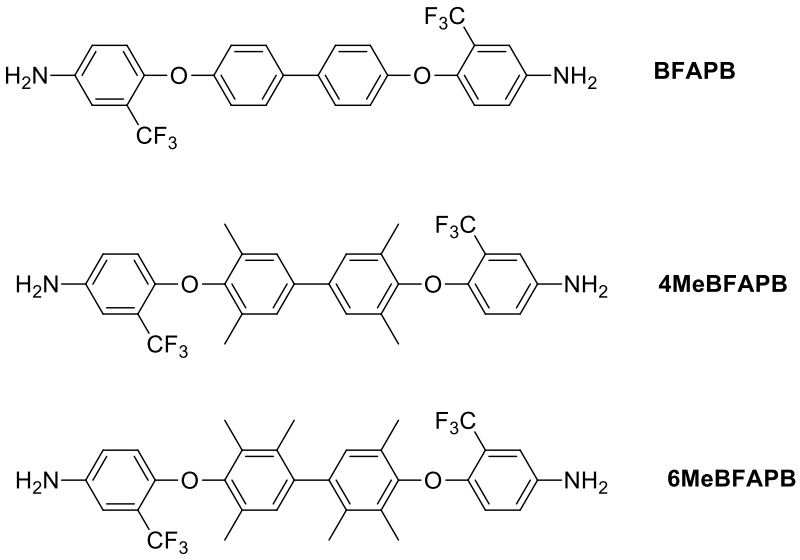

Figure 1. Chemical structure of the diamines used in this work.

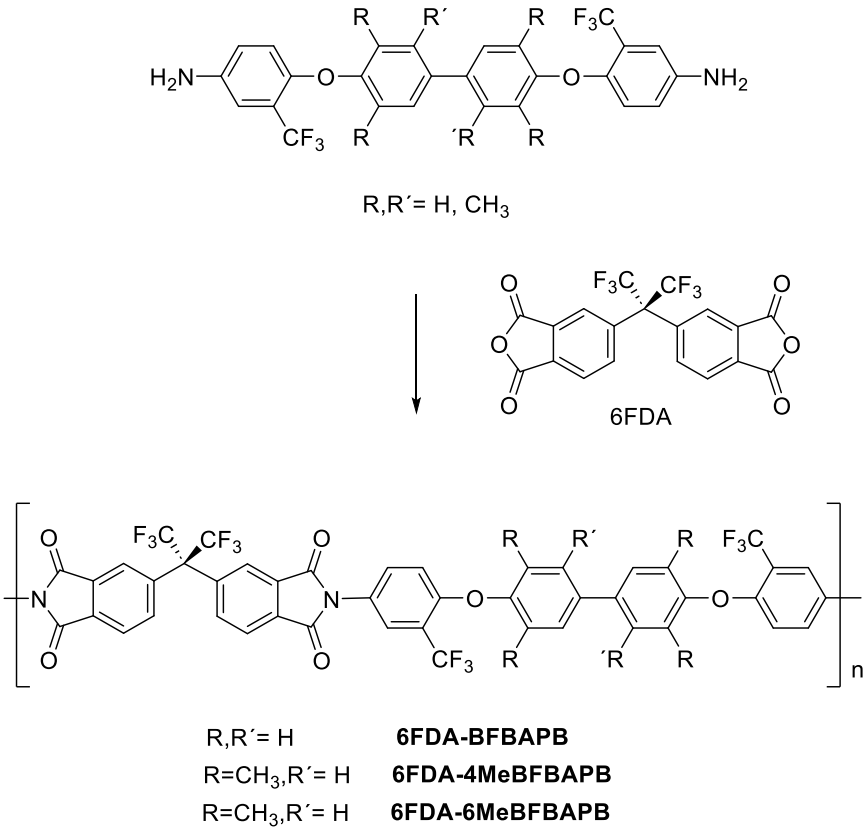

Figure 2. Synthesis of aromatic biphenyl polyimides

It should be pointed out that the synthesis of the 6FDA-BFAPB and 6FDA-4MeBFAPB polyimides has been previously described by Yang et. al[26], but no studies of these materials as gas separation membranes have been reported.

In this research, the three polyimides were tested in permeation measures with pure gases, and real gas mixtures at high pressures. A gas adsorption study of these polyimides was also carried out.

2. Experimental

2.1. Materials

1-Chloro-4-nitrobenzene 99%, bisphenol A 99%, 3,5-diaminobenzoic acid 98% (DABA), hydrazine monohydrate 98%, palladium on carbon at 10%wt, sodium chloride, chloroform, hexane, N,N-dimethyformamide (DMF), N,N-dimethylacetamide (DMA), m-cresol, ethanol, pyridine (Py), acetic anhydride, 1,4-butanediol, p-toluenesulfonic acid, xylene, potassium carbonate anhydrous, magnesium sulfate anhydrous, methanesulfonic acid, acetic acid, phosphorous pentoxide were purchased from Sigma Aldrich.

3,3',4,4'-biphenyltetracarboxylic dianhydride (BPDA) was obtained from Criskev Company Inc. 1-chloro-4-nitro-2-(trifluoromethyl)benzene 98%, 3,3',5,5'-tetramethyl[1,1'-biphenyl]-4,4'-diol 98%, 2,2',3,3',5,5'-hexamethyl-[1,1'-biphenyl]-4,4'-diol 98%, 4,4'-Bis(4-amino-2-trifluoromethylphenoxy)biphenyl 99% (BFAPB), pyromellitic dianhydride (PMDA) and 4,4'-(hexafluoroisopropylidene)diphthalic anhydride (6FDA) were obtained from Akron Polymer Systems, Akron. All the reagents were used as received, except for 6FDA, it was sublimed before use.

2.2. Monomer synthesis

The diamino monomers 4MeBFAPB and 6MeBFAPB were obtained by the similar synthetic procedures (**Scheme S1** of supporting information). By way of example, the synthesis of 4MeBFAPB is described as follows:

3,3',5,5'-tetramethyl-4,4'-bis(4-nitro-2-(trifluoromethyl)phenoxy)-1,1'-biphenyl (1)

In a 100 ml flask, 3,3',5,5'-tetramethyl[1,1'-biphenyl]-4,4'-diol (5.00 g, 20.6 mmol). 1-chloro-4-nitro-2-(trifluoromethyl)benzene (9.78 g, 43.4 mmol), potassium carbonate anhydrous (6.28 g, 45.4 mmol), and 40 ml of anhydrous DMA were added. The solution was agitated at 120°C for 4 h until the reaction was completed. The reaction evolution was followed by thin layer chromatography (TLC).

Then the reaction mixture was let to cool to room temperature and diluted with chloroform. The resultant dissolution was washed with basic water and with a saturated solution of sodium chloride. The organic phase was dried on magnesium sulfate, and it was concentrated until dry. The obtained yellow solid was washed with hexane giving the desired product (compound 1, **Scheme S1**) without any additional purification. ^{1}H NMR (300 MHz, $CDCl_3$, δ ppm): 8,64 (d, J = 2.7 Hz, 2H), 8.29 (dd, J =9.2, 2.8 Hz, 2H), 7.38 (s, 4H), 6.68 (d, J = 9.2 Hz, 2H), 2.20 (s, 12H). ^{13}C NMR (75 MHz, $CDCl_3$, δ ppm): 160.1; 149.1; 141.3; 138.6; 131.1; 129.1; 128.2; 126.5; 124.4 (c, JC-F= 5Hz); 120.5; 119.4(c, JC-F= 30Hz); 114.1. Elemental analysis $C_{30}H_{22}F_6N_2O_6$ (620.50 g/mol) calculated: C: 58.07%; H: 3.57%; N: 4.51% found: C: 57.96%; H: 3.57%; N: 4.80%. Yield: 70%; m. p. 263-265°C.

4,4'-((3,3',5,5'-tetramethyl-[1,1'-biphenyl]-4,4'-diyl)bis(oxy))bis(3-(trifluoromethyl)aniline) (4MeBFAPB)

In a three-neck flask fitted with a condenser and nitrogen flux, the dinitro compound (1) (6.0 g, 9.7 mmol), 600 mg of Pd/C as catalyst (10%), and 90 ml of absolute ethanol were added. Hydrazine monohydrate (15 ml) was slowly added for one hour to the reaction mixture. The reaction was agitated at reflux for 24 h until the TLC showed that the reaction was complete. It was cooled to room temperature and filtered through Celite® to eliminate the residues of Pd/C. The filtered solution was concentrated and precipitated in water to obtain the product (4MeBFAPB) as a white precipitate which was washed with water, then with hexane and dried under vacuum at 60°C. The purity of the product was high enough to be employed directly in the synthesis of polyimides. ^{1}H NMR (300 MHz, DMSO-d6, δ ppm): 7.48 (s, 4H), 6.95 (d, J = 2.6 Hz, 2H), 6.67 (dd, J = 2.4, 8.8 Hz, 2H), 6.20 (d, J = 8.9 Hz, 2H), 5.14 (s, 4H), 2.11 (s, 12H).^{13}C NMR (75 MHz, DMSO-d6, δ ppm): 149.5; 145.1; 143.0; 136.4; 131.0; 127.2; 123.9 (c, JC-F= 270 Hz); 118.5; 116.4 (c, JC-F= 30 Hz); 113.9; 111.7 (c, JC-F= 5 Hz). Elemental analysis $C_{30}H_{26}F_6N_2O_2$ (560.53 g/mol), calculated: C: 64.28%; H: 4.68%; N: 5.00%, found: C: 64.33%; H: 4.76%; N: 5.26%. yield: 94%. m. p. 254-256°C.

2.3. Polymer synthesis

The three polyimides (PIs) were synthesized by the reaction between the biphenyl diamines and the 6FDA anhydride via a conventional two-step procedure using chemical imidization. The typical procedure followed in this work is described below:

In a three-neck flask, fitted with a condenser, nitrogen flux, and mechanical agitation, the diamine (7.5 mmol) and 12.0 ml of DMA were added. It was agitated until the diamine was completely dissolved; then, the solution was cooled to 0°C and 6FDA (7.5 mmol) was added, followed by

addition of DMA (6.0 ml). The mixture was allowed to reach room temperature at constant agitation and, thus, the reaction was maintained for 16 h. Then, the cyclization of the polyamic acid was carried out by adding to the solution a mixture of acetic anhydride, (32.1 mmol) and pyridine (32.1 mmol). It was agitated at room temperature for 1 h, at 40°C for 1 h and, finally, at 60°C for another 1 hour. Once the solution of polyimide was cooled, it was precipitated in 750 ml of a water/ethanol (2/1) mixture. The polymer was dried at 150°C under vacuum for 16 h. The three polymers were obtained quantitatively.

2.4. Preparation of the Polymeric Membranes

The polymeric films were prepared by casting from $CHCl_3$ solutions (5% w/v). The solutions were filtered prior the casting. The solvent was allowed to evaporate slowly at room temperature giving solid films. Subsequently, the obtained films were subjected to a thermal treatment to eliminate completely the residual solvent: in vacuum 3 h at 150 °C and 1 h at 180 °C, then N_2 atmosphere was added, and the temperature protocol was 30 min at 200 °C, 30 min at 250 °C, 30 min at 300 °C and finally 5 min at 335 °C. In the last stage of the treatment, the films were heated at a temperature of 15°C over their glass transition temperatures (Tg), and then they were cooled down in the oven. In this way, it was assured that all the films had the same thermal history.

2.5. Characterization

^{1}H and ^{13}C NMR spectra were recorded on a Varian Innova 400 at 400 MHz and 75 MHz, respectively. A Perkin Elmer Fourier transform infrared spectrometer (FT-IR) with Universal ATR Sampling Accessory was used to characterize the polyimides films. The scan range was from 4000 to 650 cm^{-1}.

The inherent viscosity of polyimides was measured at 30 °C using an automated Canon-Ubbelohde suspended level viscometer with NMP as the solvent. The polymer concentration was 0.5 g/dL. Differential scanning calorimetric (DSC) data were obtained on a TA Instruments DSC Q-2000 Analyzer (TA Instruments, DE, USA). Thermogravimetric analyses (TGA) were performed on a TA Instruments Q-500 thermobalance (TA Instruments, DE, USA). Dynamic ramp scans were run at 10 °C/min under nitrogen (60 mL/min), using approximately 5 mg of sample. The mechanical properties of polymers were obtained at room temperature with an apparatus MTS Synergie 200, using samples of 5 mm x 50mm at a test speed of 5 mm/min.

Intermolecular distances of polymer membranes were determined by wide-angle X-ray scattering

(WAXS) experiments performed in reflection mode at room temperature with a Bruker D8 Advance system fitted with a Goebel mirror and a PSD Vantec detector. A Cu-Kα (wavelength λ=1.542Å) radiation source was used. A step scanning mode was employed for the detector from 2–55°, with a 2θ step of 0.024° and a scan rate of 0.5s per step. The average *d*-spacing was obtained from the Bragg's equation:

$$n\lambda = 2dsin\theta \quad (1)$$

where *d* is the d-spacing, θ is the scattering angle and *n* is an integer number related to the Bragg order.

Density was determined using XS105 Dual Range Mettler Toledo balance coupled with a density kit based on Archimedes' principle. The samples were weighed in air and into a known-density liquid (high-purity isooctane). The measurement was performed at room temperature and the density was calculated from the following expression:

$$\rho_{sample} = \rho_{liquid} \frac{W_{air} - W_{liquid}}{W_{air}} \quad (2)$$

The density data were used to evaluate chain packing using the fractional free volume (FFV), which was calculated using the following relation:

$$FFV = \frac{V_e - 1.3V_w}{V_e} \quad (3)$$

where V_e is the polymer specific volume and V_W is the van der Waals volume, which was obtained by molecular modeling applying the semi-empirical method Austin Model 1 (AM1) in the Hyperchem computer program, version 8.0.

Gas permeation properties were determined for single gas feeds using a constant volume/variable pressure apparatus at 30 °C (the device scheme is included in **Scheme S2** of supporting information). The downstream pressure was maintained below 10^{-2} mbar, while the upstream pressure was kept at 3 bar for all gases. For the measures, He, O_2, N_2, CH_4, and CO_2 were used. The purities for CH_4 and O_2 were greater than 99.95%, and the other gases were greater than 99.99%. Helium permeation tests at three upstream pressures (1, 3 and 5 bar) were carried out to verify the absence of pinholes. Permeability values for all polymers were determined from the slope of downstream pressure vs. time plotted (*dp(t)/dt*) on the steady state had been achieved, according to the expression:

$$P = \frac{273}{76} \frac{Vl}{ATp_o} \frac{dp(t)}{dt} \quad (4)$$

where A (cm^2), V (cm^3) and l (cm) are respectively the effective area, the downstream volume and the thickness of the film, T is the temperature in K, and p_o (cmHg) the pressure of the feed gas in the upstream chamber. P is usually expressed in Barrer [1 Barrer = 10^{-10}(cm^3(STP)cm)/(cm^2scmHg). The ideal selectivity for a gas pair was calculated from the ratio of their pure gas permeabilities.

$$\alpha_{A/B} = \frac{P_A}{P_B} \tag{5}$$

where P_A and P_B are the permeability coefficients of pure gases A and B, respectively.

The mixed-gas permeation properties for the polymers were made at a temperature of 35°C, and the employed composition of the mixture of gases was CO_2/ CH_4 (50/50). The device scheme is included in **Scheme S3** of supporting information).

The solubility coefficients and dual-mode sorption were fitted to the following equation.

$$S = \frac{C}{p} = k_D + \frac{C_H' b}{1 + bp} \tag{6}$$

Where C is the adsorption quantity at equilibrium (cm^3(STP)·g^{-1}); p is the equilibrium pressure (kPa); K_D is Henry's law constant (cm^3·g^{-1}·kPa^{-1}), b is the affinity coefficient (kPa^{-1}), and C'_H is Langmuir coefficient (cm^3·g^{-1}).

$$C_D = K_D \times p \tag{7}$$

where K_D is the Henry solubility coefficient, p is the pressure exerted by the gas, and C_D is the concentration of the dissolved gas. K_D represents the amount of penetrant gas dissolved in the matrix and depends on the temperature, the gas nature and the matrix.

The Langmuir-type adsorption is typical in the phenomena of solubility of gases in porous solids. In this type of adsorption, the solubility increases as the pressure rises until the concentration of the absorbed gas reaches an asymptotic value. In this case, the process is described by the following expression:

$$C_H = \frac{C_H' bp}{1 + bp} \tag{8}$$

where C_H is the concentration at equilibrium, C'_H is the parameter of capacity, related to the excess volume present in the matrix, and b is denominated the affinity constant and represents the absorption affinity for a given polymer-gas system.

As we have seen previously, the solid state of the glassy polymers is defined as a non-equilibrium state between two components; a hypothetical liquid state and a solid, in such a way that the gas adsorption in those materials is considered as the sum of the two previous types of adsorption:

$$C = C_D + C_H \tag{9}$$

Scheme S4 shows the system used to measure the adsorption of gases[27]. The system consists of two chambers of known volume (VA and VB) connected by a valve. Chamber B is the chamber of charge of the gas and chamber A is where the sample is introduced (between 0,5 – 1 g). Each chamber is connected to an absolute pressure transducer (pA and pB) that registers the changes in the pressure produced during the test. The calibration of the two transductors is made in such a way that both show the same data for a determined pressure. Furthermore, the system is controlled at a constant temperature, in this case, of 35°C.

The methodology to carry out the measurements is described below:

First, a sample is introduced (approximately 1 g of the membrane) into chamber A and it is degassed maintaining the system under vacuum for 12 h. Then, chamber A is isolated and subsequently, the gas is loaded into chamber B at the desired pressure.

Once the pressure in the charge chamber stabilizes, the valve that connects both chambers is opened for a very short time, so the gas expands to chamber A, initiating the measurement until reaching equilibrium (i.e., when the pressure in chamber A barely changes through time). After the measurement finishes and the pressure in chamber A is constant, chamber B is loaded at the next pressure for measurement. The gas expands to chamber A, and we wait one more time until reestablishing equilibrium, and so on.

3. Results and Discussion

The route for the synthesis of 4MeBFAPB and 6MeBFAPB diamines is presented in **Scheme S1**. The synthesis comprises two steps: in the first one, the corresponding diols reacted with 1-chloro-4-nitro-2-(trifluoromethyl)benzene via a nucleophilic aromatic substitution to obtain the dinitro precursors (1) and (2); in the second, the reduction was performed by two different ways (i/ii) to obtain the diamines.

Reduction is a key process in this synthesis since the purity of the monomers is essential for further polymerization. Therefore, the synthetic protocol that showed the best yield and/or the cleanest reactions was chosen. This optimal method (i or ii) is described below for each one of the diamines. The syntheses of the intermediates were also modified with respect to the procedure reported in the literature[26,28] for solvents, reaction times, etc., and, subsequently, the intermediate nitro-compounds were obtained in higher yields.

3.1. Synthesis and Characterization of Monomers

The synthesis of the diamines was carried out by high-yield reactions (higher than 70% in all steps). The dinitrated intermediates demonstrated different reactivities and solubilities and, therefore, the conditions had to be optimized in each case. Such, 4MeBFAPB of high purity was readily obtained practically without any additional purification in the reduction step. In contrast, dinitro precursor of 6MeBFAPB was less soluble and required longer reaction times and a different solvent to obtain a high yield.

The reduction method employed for the synthesis of 4MeBFAPB, using hydrazine and Pd/C, resulted in a clean reaction, without the presence of subproducts derived from the partial reduction of the dinitro precursor. On the contrary, in the case of 6MeBFAPB, the reaction carried out under the same conditions led to diverse subproducts of partial reduction (mostly mono-reduced compound), so it was not possible to obtain the diamine with acceptable purity and/or yield. Therefore, we decided to perform the reduction in a hydrogenation system, as described in the Experimental section, at a pressure of 3 atm (1atm is equivalent to 1.013 bar). Through this procedure, the diamine in excellent yield and purity was obtained without the presence of reaction subproducts.

In **Figure S1** and **Figure S2**, the ^{1}H-NMR spectra of the dinitrated intermediate (1) and the tetramethylated diamine 4MeBFAPB, respectively, are shown. All signals correspond to those previously reported in the literature[26,28]. **Figure S3** shows the ^{1}H-NMR spectrum of the dinitrated intermediate (2), with 6 methyl groups, all the signals agree with the proposed structure. It was observed that methyl groups presented 4 different signals; two of them corresponded to the exterior CH_3 (6H), and the other two corresponded to the interior methyl groups (3H). Likewise, two kinds of signals corresponding to the positions d (2 singlets, d and d') and c (2 doublets, c and c') were observed. This should be expected since the molecule is asymmetric, and the rotation around the central C-C bond of the biphenyl may be hindered by the *ortho* substituents, which results in an impediment to the interconversion of the conformers. **Figure S4** shows the ^{1}H-NMR spectrum of

6MeBFAPB diamine. In this spectrum, we can again observe two signals for the protons in positions d (d and d') and two for the internal methyl's.

AM1 molecular models for the diamines BFAPB (top), 4MeBFAPB (middle), and 6MeBFAPB (bottom) are shown in **Figure 3**. The dihedral angle formed by the aromatic rings of the biphenyl unit is 41° in diamines BFAPB and 4MeBFAPB. In the case of the 6MeBFAPB diamine, the dihedral angle changes to 74°. It means that the aromatic rings of the biphenyl group in this diamine are located in almost orthogonal positions, which is due to the steric hindrance between the methyl groups in positions 2 and 2'.

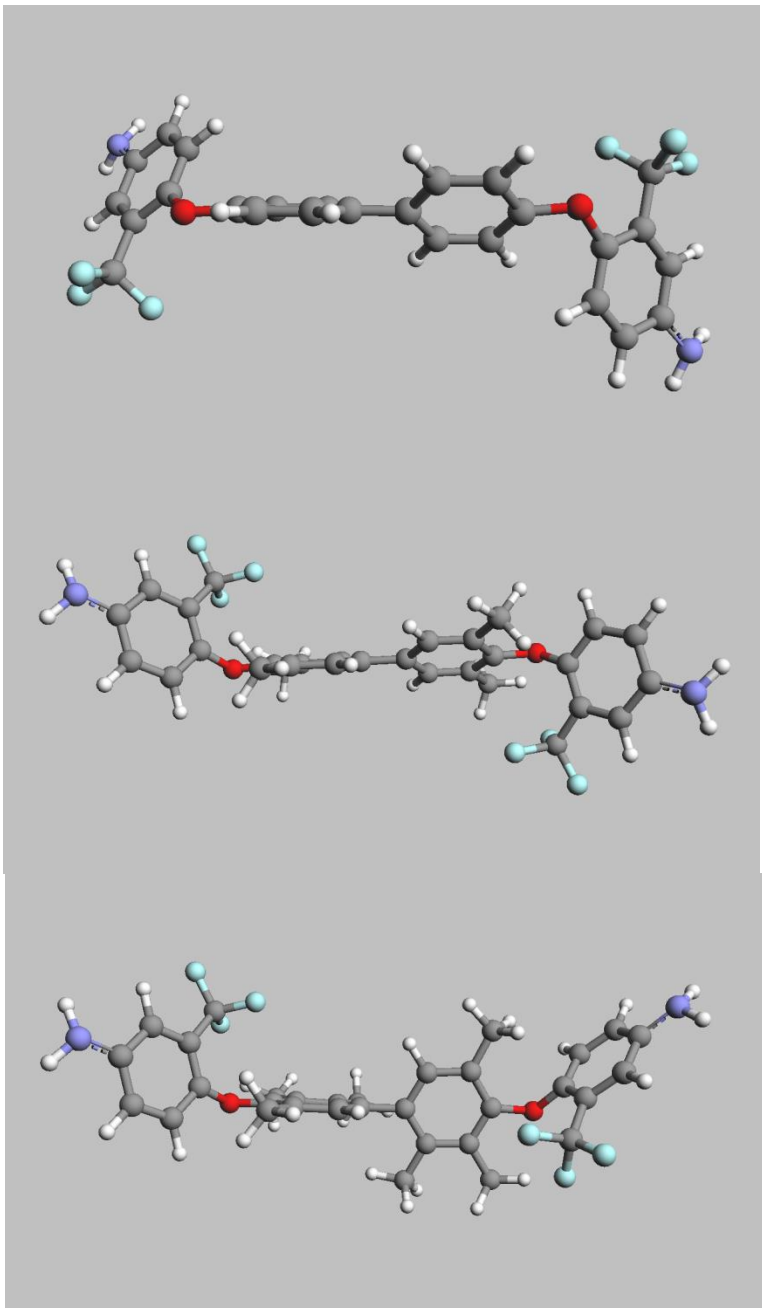

Figure 3. Molecular modeling (AM1) of BFAPB (top), 4MeBFAPB (middle), and 6MeBFAPB (bottom)

3.2. Polymer synthesis

The synthesis of polyimides was carried out via a conventional two-step procedure using chemical imidization to convert the polyamic acid to the corresponding polyimide. The polymerization reactions were quantitative in both steps.

The BFAPB and 4MeBFAPB diamines led to polyimides that precipitated in the shape of a tangle, as shown in **Figure S5** (left); while the polyimide from 6MeBFAPB precipitated in the shape of strings (right) and its apparent toughness was lower than for the other two polyimides.

Numerous polymerization reactions were performed to obtain 6FDA-6MeBFAPB with high enough molecular weight to form films with good mechanical properties. It should be noted that the variations in the conditions of the reaction such as reaction time, solvents, etc., did not show good results. Finally, the diamine was heated at 200°C in vacuum for 2 h and immediately reacted with the 6FDA dianhydride. Once the dianhydride was dissolved, the solution was slightly heated to increase reactivity. Using this synthesis method, it was possible to obtain a polymer with a sufficiently high molecular weight to form a film with acceptable mechanical properties.

To study the anomalous behavior of the diamine 6MeBFAPB in the polycondensation reaction (lower molecular weight polymer than those when the other two diamines were used), the Mulliken charges (electron densities) on the amino nitrogen, and the energies of the HOMO, E_{HOMO}, of the three diamines orbitals were calculated (**Table S6**, computational methods are described in the supporting information S5 section). Since this orbital energy provides quantitative information on the reactivity of the aromatic diamines when they react with a certain dianhydride electrophile by determining the frontier orbital energy gap, ($E_{HOMO(diamine)}$-$E_{LUMO(dianhydride)}$), so that the smaller the gap, the higher the reactivity[29–31]. It was observed that the electron densities on the nitrogen atoms were similar for the three monomers. Regarding orbital HOMO energies, it was found that the highest HOMO orbital energy (-8.60 eV (AM1 method) and -5.35 eV (DFT method)) corresponded to BFAPB. For the other two diamines, the E_{HOMO} values were practically the same, no matter the quantum-mechanics method used, indicating that both monomers were equivalent in terms of their electronic reactivity.

Observing the geometry of the three monomers (**Figure 3**), it can be seen that the orthogonality of the aromatic rings in the 6MeBFAPB diamine should modify the conjugation of the biphenyl unit, which would bring modifications in the electronic characteristics of the amino group. The CF_3 group not only brings electronic modifications, but as shown in the structures of **Figure 3**, the interaction between the methyl groups of the 4MeBFAPB and 6MeBFAPB diamines with the trifluoromethyl group produces a conformational change that is not observed in the BFAPB diamine. Thus, the dihedral angle (DH) values between the C1 of the biphenyl ring, the oxygen, the C1 of the ring bearing the amino group, and the C6 of that same ring, *ipso* to the trifluomethyl group are very different between BFAPB and the biphenyl monomers with methyl groups (DH_{BFAPB}=114.5º, $DH_{4MeBFAPB}$ =163.8º, and $DH_{6MeBFAPB}$ =168.0º). That is, the DH of the methyl monomers are completely similar,

with a value close to 180º indicating that the electronic conjugation between the biphenyl unit and the aromatic ring having the amino group is low. To demonstrate this idea, we modeled 3-trifluoromethyl aniline, a compound where the biphenyl group has been exchanged for an H atom, observing that in this case its HOMO energy is -5.63 eV (DFT), a lower value than the 3 monomers, but closer to 4MeBFAPB and 6MeBFAPB.

Thus, the polycondensation differences observed between 4MeBFAPB and 6MeBFAPB should not be associated with electronic effects, but rather with differences in the conformations of the macromolecular chains of these two polymers, or to a lower purity (although the purification of the monomers was very exhaustive) of the 6MeBFAPB monomer.

3.3. Characterization of Polymers and Polymeric Membranes

FT-IR spectra of PIs are displayed in **Figure 4**. All PIs showed the characteristic imide group bands at 1780 y 1730 cm^{-1} (asymmetrical and symmetrical C=O stretching, respectively), 1380 cm^{-1} (C-N stretching), 1100 and 725 cm^{-1} (deformation of the imide cycle), as well as the different bands in the region 1100-1300 cm^{-1} due to the C-O and C-F stretching. Concerning the methylated PIs, the small peaks between 2600 and 3000 cm^{-1} were useful to determine the substitution in aromatic rings. Also, some variations were observed in the bands corresponding to the skeletal vibrations (aromatic C-C tensions) at 1490 cm^{-1} due to the different substitutions and the existence of different types of symmetry.

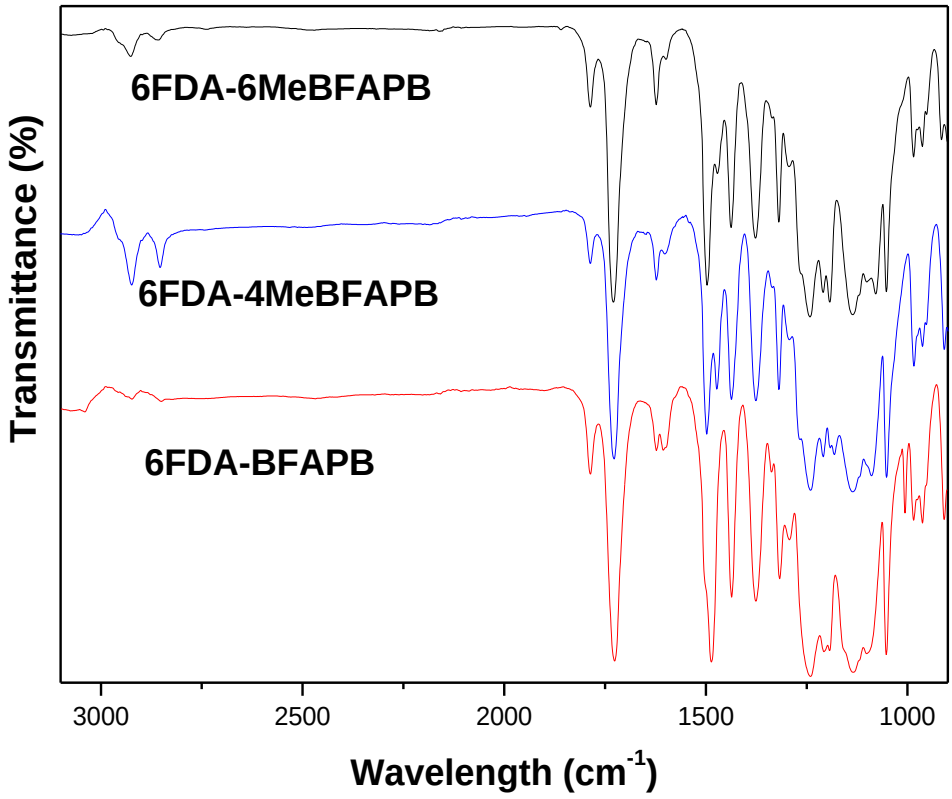

Figure 4. ATR-FTIR spectra of the biphenyl PIs

As can be observed in **Table 1**, the synthesized polyimides presented excellent solubilities at room temperature, not only in the solvents traditionally used for the preparation of membranes but also in common organic solvents like $CHCl_3$ and THF.

Table 1. Solubility of the PIs at room temperature

Polymer	**$CHCl_3$**	**THF**	**DMA**	**NMP**	***m*-Cresol**
6FDA-BFAPB	+ +	+ +	+ +	+ +	+ +
6FDA-4MeBFAPB	+ +	+ +	+ +	+ +	+ +
6FDA-6MeBFAPB	+ +	+ +	+ +	+ +	+ +

Thermogravimetric curves of the PI membranes in a nitrogen atmosphere are depicted in **Figure 5**. It can be observed that there is no weight loss due to residual solvent evaporation and/or cyclization until the degradation temperature of the polymer, confirming the complete cyclization of the imide in the polymer.

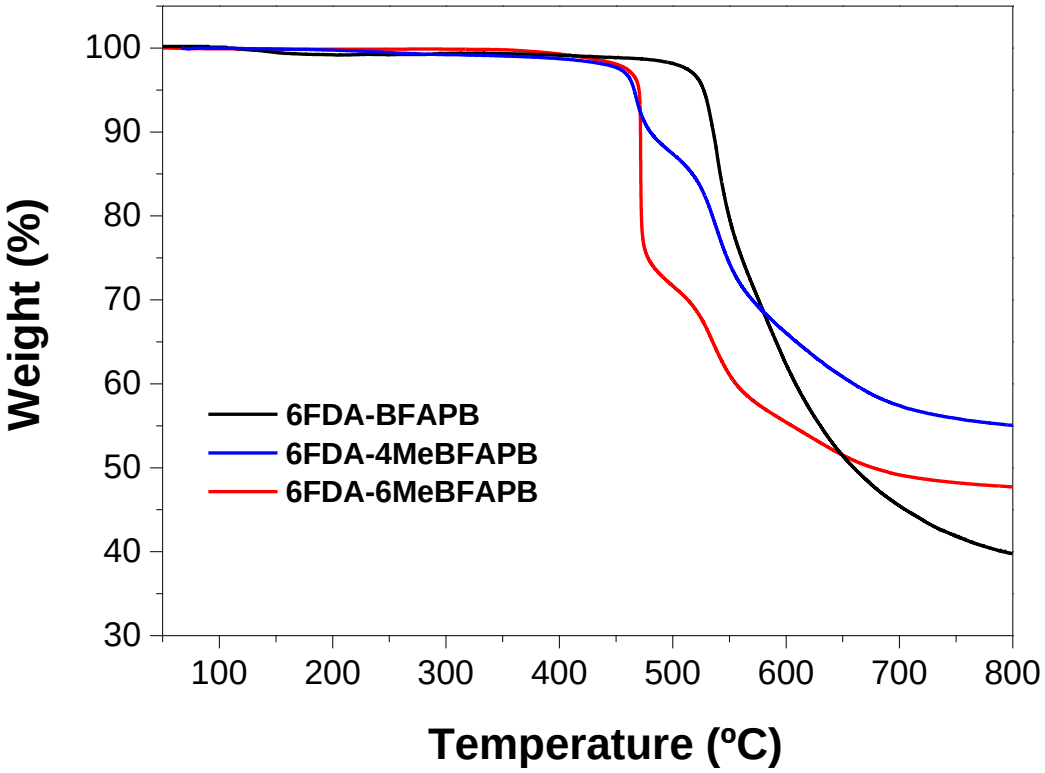

Figure 5. TGA curves of biphenyl PIs

Table 2 compiles the degradation onset temperatures (Td) and the char yields at 800°C of these PIs. In general, all of polyimides presented high thermal resistance. The Td of 6FDA-BFAPB was 70°C higher than that of the methylated polyimides. The char residues were high, which should be expected due to the aromatic and heterocyclic character of these materials.

Table 2. Thermal decomposition data and Tg of the biphenyl PIs heated to 800 °C in a nitrogen atmosphere.

Polymer	**Td (°C)**	**R_C (%)**	**Tg (°C)**
6FDA-BFAPB	530	40	265
6FDA-4MeBFAPB	460	55	320
6FDA-6MeBFAPB	460	45	320

On the other hand, the thermogram of 6FDA-BFAPB showed a single step in its degradation, while the two-step character of the degradation was observed for the methylated polyimides. The first step

of these thermograms is rather associated with the loss of the methyl substituents before the decomposition of the main polymeric chains. However, the weight loss detected during the first step was bigger than the total amount of methyl groups in the polymer (4MeBFAPB: theoretical 6%, experimental 11%; 6MeBFAPB: theoretical 9%, experimental 23%), so it can be assumed that the loss of $–CH_3$ induces other processes of partial degradations.

The carbon residues were high, that should be expected due to the aromatic and heterocyclic character of these materials. Interestingly, that higher char yields were detected for the methylated polyimides (**Table 2**), that may be explained by a series of radical reactions caused by release of methyl radicals that resulted in aromatic crosslinking and, therefore, increase in carbon residue. The highest chair yield of 55 % at 800 C noted for 6FDA-4MeBFAPB was rather related to its higher molecular weights.

The glass transition temperatures (Tg) of the synthesized PIs in the form of films are presented in **Table 2**. The methylated polyimides exhibited the same Tg's, while Tg of 6FDA-BFAPB was 55°C lower. This fact could be associated with higher rigidity of the chain introduced by the methyl substituents, that partially confirmed by molecular models for the diamines discussed above; the rotation around the ether linkage is more restricted in the monomers with methyl groups. The *ortho*-positioned groups should imped the rotation stronger than those in *metha*-position, that is probably why 6FDA-4MeBFAPB and 6FDA-6MeBFAPB exhibited the same Tg's.

Data in **Table S1** show that the films of 6FDA-BFAPB and 6FDA-4MeBFAPB presented good mechanical properties, with Young's modulus and tensile strength greater than 1.6 GPa and 66 MPa, respectively. The 6FDA-6MeBFAPB films exhibited values of resistance to traction and elongation at break lower than those of 6FDA-BFAPB and 6FDA-4MeBFAPB. This film had also the lowest value of elongation at break, less than 5%, while the other PI films had values greater than 10%. It may indicate that the molecular weight of 6FDA-6MeBFAPB is lower than those of another two PIs, which agrees with the data on the molecular weights discussed below. However, all films present mechanical properties superior to the necessary to be employed as separation membranes at high pressures.

Figure 6 shows the diffraction profiles for the three synthesized PIs. In all of them, the amorphous nature of these polymers was observed. At first sight, it is evident that the diamine affects the chain packing. It has been observed that the introduction of methyl groups produced a small displacement of the maximum of the highest intensity towards the lowest angles. Thus, the most probable

intersegmental distance was 5.4 Å (2θ= 16.5°) for 6FDA-BFAPB and approximately 6 Å (14.9°) for two other methyl-substituted PIs.

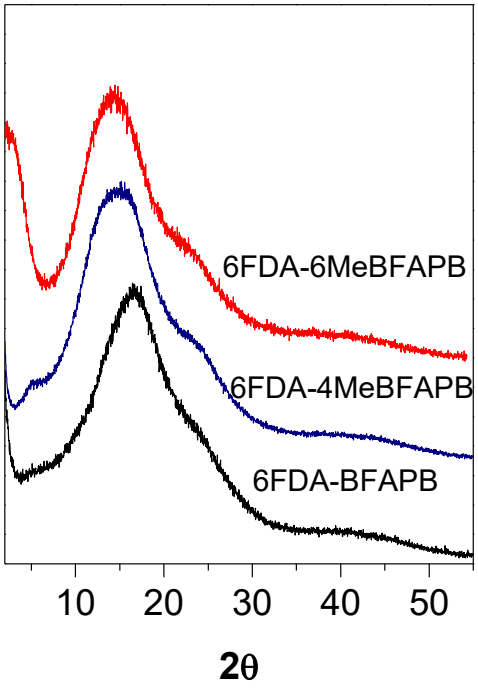

Figure 6. Diffractograms of the biphenyl PIs

On the other hand, the presence of methyl groups in the biphenyl unit widened the amorphous halo at the zone of the low angles, which indicates a higher contribution of these groups to the intersegmental distances. The presence of methyl groups close to the biphenyl bond hinders the rotational angle and promotes a less packed structure as can be seen in **Figure 6**. This could be related to a higher fractional free volume for the substituted PIs. Nevertheless, despite these PIs having different numbers of methyl groups, their diffraction profiles did not show important changes.

Table 3 lists the inherent viscosities and the average molecular weights (Mw and Mn), as well as the dispersity index (ID) determined by GPC. The 6FDA-6MeBFAPB polyimide presented an Mw much lower than the other two polyimides. In addition, for 6FDA-BFAPB, the Mw was half of that of 6FDA-4MeBFAPB, although its polydispersity was considerably lower. The inherent viscosities for 6FDA-BFAPB and 6FDA-4MeBFAPB were much higher than the values of inherent viscosity reported in the bibliography (0.92 and 0.74 dL g-1, respectively)[26,28], which suggests the achievement of molecular weights considerably higher with the polymerization conditions in this work.

Table 3. Inherent viscosity, average absolute molecular weights, and dispersity indexes of the biphenyl PIs.

Polymer	[η] (dL·g^{-1})	M_n	M_w	DI
6FDA-BFAPB	1.50	148.900	240.500	1.6
6FDA-4MeBFAPB	1.65	174.700	522.500	3.0
6FDA-6MeBFAPB	0.54	36.500	76.700	2.1

The fractional free volume of the synthesized polyimides (FFV) was estimated through the combination of measurements of density and theoretical determinations of the van der Waals volume, and the obtained data are given in **Table S2**. As expected, the PIs derived from the methylated diamines presented higher FFV than those derived from BFAPB. 6FDA-6MeBFAPB polyimide showed the highest value, which agrees with the biggest number of methyl groups introduced.

3.4. Gas Separation Properties

3.4.1. Permeability Coefficient

In **Table 4** the data of permeability (P) and ideal selectivity (α) for O_2/N_2 and CO_2/CH_4 pairs of gases are displayed. It is notable that the incorporation of the methyl groups in the repetitive unit results in a significant increase in the permeability for all gases.

Table 4. Permeability Coefficients and Ideal Selectivity (α) of the biphenyl PIs.

Polymer	P_{He}	P_{O_2}	P_{N_2}	P_{CH_4}	P_{CO_2}	α_{O_2/N_2}	α_{CO_2/CH_4}
6FDA-BFAPB	57	5.5	1.1	0.82	25	5.0	31
6FDA-4MeBFAPB	160	30	6.9	5.2	140	4.3	27
6FDA-6MeBFAPB	180	36	8.9	5.2	130	4.0	25

[a] Permeability in barrers. 1 barrer = 10^{-10} cm^3 (STP) cm/cm^2 s cmHg. Measurement conditions: 3bar, 30°C

For the O_2/N_2 pair of gases, the increase in the permeability of 6FDA-4MeBFAPB vs 6FDA-BFAPB was 450 % for O_2 and 500 % for N_2, with a reduction in the O_2/N_2 selectivity of 15 %. For 6FDA-6MeBFAPB vs 6FDA-BFAPB, the increase in the permeability was 550 % for O_2 and 700 % for N_2, and the O_2/N_2 selectivity was reduced by 20%. Comparing the two PIs with methyl groups, 6FDA-6MeBFAPB exhibited an increase in permeability of 20 % for O_2 and 30 % for N_2, which agrees with the highest FFV presented by this PI. Nevertheless, the selectivity did practically not change.

In the case of the CO_2/CH_4 pair of gases, a significant improvement in the permeability of CO_2 and CH_4 was noted for PIs with methyl groups. The increase in CO_2 permeability was 460 % for 6FDA-4MeBFAPB and 420 % for 6FDA-6MeBFAPB with respect to that for 6FDA-BFAPB; while for CH_4, the increase was 530 % for both methylated PIs. However, the CO_2/CH_4 selectivity decreased with respect to that found in 6FDA-BFAPB (a decrease of 13% and of 20% for 6FDA-4MeBFAPB and 6FDA-6MeBFAPB, respectively).

Figure S6 and **Figure 7** show these results on Robeson-type graphs of selectivity vs permeability to evaluate the productivity of the membranes studied for the separation of O_2/N_2 and CO_2/CH_4. The Robeson limits of 1991 and 2008 and 6FDA-6FpDA polyimide, which contains hexafluoroisopropylidene units in both dianhydride and diamine fragments, are included as material for reference[32].

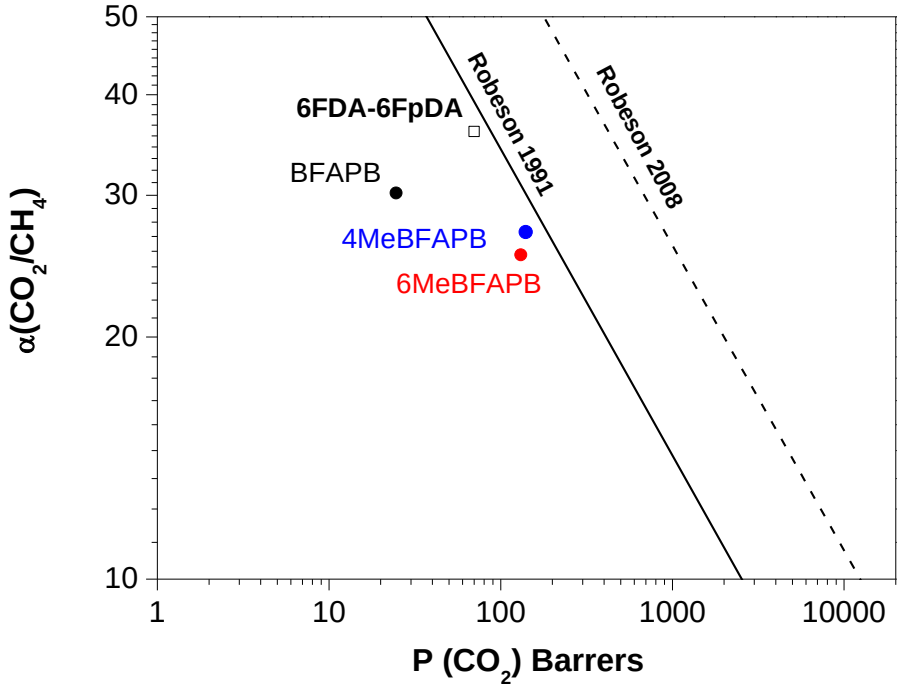

Figure 7. Representation of Selectivity vs Permeability for CO_2/CH_4

For the O_2/N_2 pair, it was observed that the presence of 4 or 6 CH_3 groups in the repetitive unit resulted in similar productivities of the membranes regarding their proximity to the 1991 Robeson limit.

The increase in these membranes' productivity was also noted for the CO_2/CH_4 gas pair although, in this case, 6FDA-4MeBFAPB laid a bit closer to the Robeson limit.

It can therefore be concluded that the introduction of methyl groups into the biphenyl unit produced an important increase in the membranes' permeability. Although a loss in selectivity was also observed, it was minor in comparison with the enhancement in the permeability. Thus, the strategy of introducing elements that restrict molecular mobility and hinder chain packing could be considered successful in improving the gas transport properties of the polymers.

3.4.2. Diffusion and Solubility Coefficients

To get deeper insight into the mechanism of gas transport of the biphenyl PI membranes, the values of diffusion and solubility were determined as described in equation 1 and given in **Table 5** and **Table S3**, respectively. The diffusion selectivity (αD) and solubility (αS) were also included in these Tables.

Table 5. Coefficients of diffusion (D)[a] and selectivities by diffusion (αD) of the biphenyl PIs

Polymer	D_{O_2}	D_{N_2}	D_{CH_4}	D_{CO_2}	$\alpha D_{(O_2/N_2)}$	$\alpha D_{(CO_2/CH_4)}$
6FDA-BFAPB	4.4	1.1	0.27	1.7	4.0	6.3
6FDA-4MeBFAPB	15	4.7	1.3	7.7	3.2	5.8
6FDA-6MeBFAPB	16	4.3	1.3	8.1	3.7	6.2

[a] $D \cdot 10^{-8}$ cm^2/s

For each PI, the diffusion coefficient decreased when the kinetic diameter of the gases decreased, except for CO_2. In general, the diffusion coefficient increases with the increase of the FFV of the polymer. Indeed, such a phenomenon was observed in the PIs studied; the methylated PIs having higher FFV exhibited higher diffusions. Regarding solubility, CO_2 was the most soluble gas in all cases, while O_2 and N_2 present similar values. Therefore, the increase in permeability was mainly due to the increase in the diffusive component.

3.4.3. Study of Permeability for Real Gas Mixtures

All membranes were tested for separation of real gas mixtures. The measurements were performed at different feed pressures under conditions as similar as possible to those used at the industrial level (3-25 bar). At the same time, some measurements were also performed at different pressures (3-10 bar) in a pure gas system with the objective of comparing how the materials behave in both systems,

especially in terms of resistance to plasticization in different environments (pure gases or real gas mixtures).

Table 6. Gas permeabilities[a] and selectivities at 35°C for pure gases and real gas mixtures at different pressures[b] for 6FDA-BFAPB membrane.

Pressure	$P_{(CO_2)pure}$	$P_{(CH_4)pure}$	$\alpha_{(CO_2/CH_4)pure}$	$P_{(CO_2)mix}$	$P_{(CH_4)mix}$	$\alpha_{(CO_2/CH_4)mix}$
3	26	0.82	32	28	0.80	35
5	26	0.83	31	27	0.67	40
7	25	0.78	32	26	0.63	41
10	25	0.77	32	25	0.61	40
15	-	-	-	24	0.62	38
20	-	-	-	23	0.58	39
25	-	-	-	22	0.58	38

[a] Permeability in barrer. 1 barrer = 10^{-10} cm^3 (STP) cm/cm^2 s cmHg.; [b] Pressure in bar

Table 6 shows the data on permeability and selectivity in pure gases and mixture gases for 6FDA-BFAPB membrane. It is observable that the permeabilities of both gases, CO_2, and CH_4, tend to decrease when increasing the feed pressure, following the usual behavior of glassy polymers[33–35]. For pure gases, the permeability variations were small, approximately 5% for both gases, in the measurement interval (0 – 10 bar). Nevertheless, for the CO_2/CH_4 mixture, the permeability decreased by 12% for CO_2 and 31% for CH_4 in the same interval of pressure. It should be pointed out that the permeability for CO_2 was similar for the pure gas and for the mixture of gases in that interval, while the permeability for CH_4 was lower for the mixture, which was reflected in the higher values of CO_2/CH_4 selectivity in the mixture of gases[36].

Figure S7 shows graphically the variation of permeability for pure CO_2 and the CO_2/CH_4 mixture, depending on the feed pressure. In the case of gas mixtures, the measurements were carried out in a wider interval of feed pressure but no minimum that could be related to the pressure of plasticization was detected [37,38].

Table 7 and **Table 8** show data on permeability and selectivity for 6FDA-4MeBFAPB and 6FDA-6MeBFAPB membranes, respectively. The measurements on these polyimides could be performed at higher pressures (up to 32 bar).

Table 7. Gas permeabilities[a] and selectivities at 35°C for pure gases and real gas mixtures at different pressures[b] for 6FDA-4MeBFAPB membrane

Pressure	$P_{(CO_2)pure}$	$P_{(CH_4)pure}$	$\alpha_{(CO_2/CH_4)pure}$	$P_{(CO_2)mix}$	$P_{(CH_4)mix}$	$\alpha_{(CO_2/CH_4)mix}$
3	140	5.9	24	135	6.4	21
5	136	5.7	24	126	5.2	24
7	131	5.6	23	121	4.9	25
10	128	5.4	24	114	4.7	24
15	-	-	-	110	4.6	24
20	-	-	-	107	4.4	24
25	-	-	-	104	4.7	22
28	-	-	-	111	4.7	24
32	-	-	-	110	4.8	23

[a] Permeability in barrer. 1 barrer = 10^{-10} cm^3 (STP) cm/cm^2 s cmHg.

[b] Pressure in bar

The permeability values for 6FDA-4MeBFAPB membrane decreased by approximately 10% for pure gases, CO_2 and CH_4, in the measurement interval (0 – 10 bar). The CO_2/CH_4 selectivity remained virtually constant in the entire interval of pressures, $\alpha CO_2/CH_4$=24. In the measurements with mixtures of gases, a decrease in the permeability with the pressure was detected as well, by 30% for CO_2 and by 45% for CH_4. The selectively barely changed with the pressure and was similar to that of pure gases. For this membrane, the permeabilities for CH_4 and CO_2 in the gas mixture were lower than that for pure gases. The values of permeability for CO_2 vs feed pressure obtained for pure gases and real gas mixtures for 6FDA-4MeBFAPB membrane are plotted in **Figure 8**. In the case of the mixture of gases, the curve shows a minimum of around 25 bar; this value could be assigned to the plasticization pressure for 6FDA-4MeBFAPB.

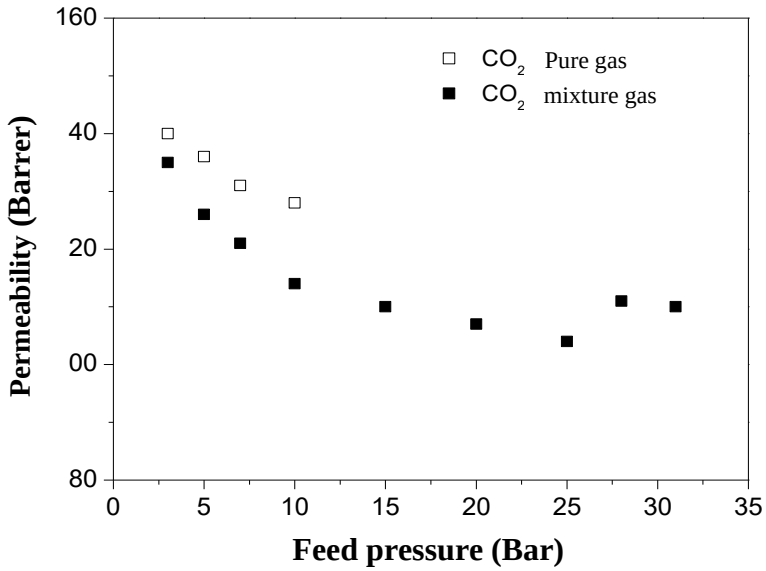

Figure 8. Permeability CO_2 vs feed pressure for the membrane 6FDA-4MeBFAPB

In **Table 8**, the data on permeability and selectivity for 6FDA-6MeBFAPB membrane are compiled. Unlike the other membranes, where the permeability decrease was the same for both pure gases, for this membrane, the permeability for CH_4 diminished by 40% and for CO_2 by 15% with an increase of the feed pressure. Consequently, the membrane selectivity increased with the pressure.

Table 8. Gas permeabilities[a] and selectivities at 35°C for pure gases and real gas mixtures at different pressures[b] for 6FDA-6MeBFAPB membrane.

Pressure	$P_{(CO_2)pure}$	$P_{(CH_4)pure}$	$\alpha_{(CO_2/CH_4)pure}$	$P_{(CO_2)mix}$	$P_{(CH_4)mix}$	$\alpha_{(CO_2/CH_4)mix}$
3	120	5.8	21	141	6.7	21
5	112	4.8	23	128	5.1	25
7	109	4.3	25	122	5.2	24
10	105	4.1	26	114	5.0	23
15	-	-	-	109	5.5	20
20	-	-	-	104	4.9	21
25	-	-	-	101	4.4	23
28	-	-	-	99	4.3	23
32	-	-	-	98	4.2	23

[a] Permeability in barrer. 1 barrer = 10^{-10} cm^3 (STP) cm/cm^2 s cmHg.

[b] Pressure in bar

For the mixture of gases, a decrease in the permeability of 25% for CO_2 and by 35% for CH_4 in the interval 0-10 bar was detected, but in the entire measurement interval, the drop in the permeability was by 40%, and by 50%, respectively. It should be highlighted that the permeability values for the mixture of gases were higher than those for pure gases. Concerning selectivity, no clear tendency was observed in either cases; for pure gases and gas mixtures.

The permeability values for CO_2 vs the feed pressure for 6FDA-6MeBFAPB membrane are plotted in **Figure S8**. In this case, the curve did not show a minimum in the pressure measurement interval (3-32 bar), as it occurred with 6FDA-4MeBFAPB membrane. Thus, it can be concluded that 6FDA-6MeBFAPB membrane does not plasticize in the measured pressure interval (3-32 bar).

3.4.4. Solubility/Adsorption of Gases

The measurements of adsorption were made for the following pure gases: O_2, CH_4, and CO_2. Due to time limitations, N_2 was not tested since these measurements are slower (2-3 weeks for each membrane). **Figure 9** and **Figure S9** show the concentration of adsorbed gas vs fugacity of the tested gas for 6FDA-BFAPB, 6FDA-4MeBFAPB, and 6FDA-6MeBFAPB membranes.

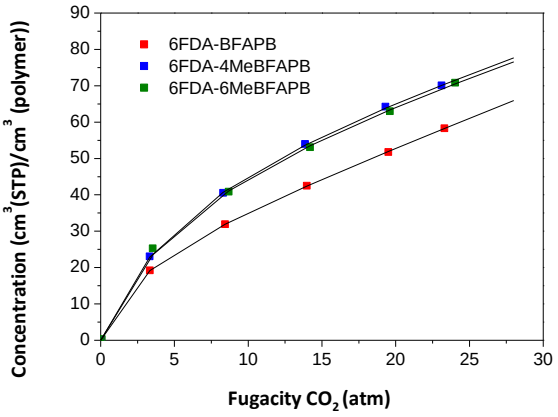

Figure 9. Isotherms of the gases tested at 35°C for the PIs' membranes. The solid lines are the adjustments to the dual-mode sorption model. (1 atm is equivalent to 1.013 bar)

It can be seen from **Figure 9** that the concentration of the gases increases as the gas fugacities increase. In general, the isothermal curves, for all gases, are concave towards the x-axis in the interval of low pressures and get more linear in the interval of high pressures, which is typical in glassy

polymers. On the other hand, it is also observed the concentration of the gas absorbed in equilibrium at a given pressure depends on the nature of the gas and is higher for the gas with the higher critical temperature: CO_2 (304 K) >CH_4 (191 K) >O_2 (150 K).

From the adjustment of each isotherm to the dual-mode sorption model (equation 6) by non-linear regression methods, the corresponding parameters K_D, C'_H, and b were determined and their values are given in **Table S4**, **Table S5**, and **Table 9** for O_2, CH_4, and CO_2 isotherms.

It is worth mentioning that the adjustment of the O_2 isotherm for 6FDA-6MeBFAPB membrane is not shown because of the high level of uncertainty arising from the low value of saturation of this gas, which is the most similar to an ideal gas among the three ones.[39]

Table 9. Parameters of the dual-mode sorption model (equation 6) for CO_2

Polymer	K_D [a]	C'_H [b]	b [c]
6FDA-BFAPB	1.56±0.02	24.2±0.5	0.41±0.02
6FDA-4MeBFAPB	1.24±0.09	52±3	0.17±0.02
6FDA-6MeBFAPB	1.23±0.09	43±2	0.26±0.02

Units: [(a)] cm^3(STP)/(cm^3(polymer)atm); [(b)]cm^3(STP)/cm^3 (polymer); [(c)] 1/atm; [(d)] cm^3(STP)/(cm^3(polymer)atm). (1 atm is equivalent to 1.013 bar)

Figure 10 and **Figure S10** show the solubility coefficients depending on the gas fugacity for 6FDA-BFAPB. 6FDA-4MeBFAPB. and 6FDA-6MeBFAPB membranes. As can be seen from this Figure. solubilities of all gases were higher in the methylated membranes. 6FDA-4MeBFAPB and 6FDA-6MeBFAPB. than in 6FDA-BFABP. while a little difference was noted between solubilities in the former membranes.

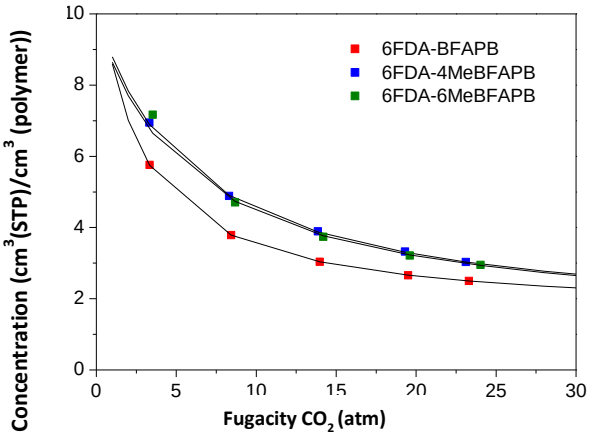

Figure 10. Isotherms of solubility vs fugacity to a determined gas for the PIs membranes. The solid lines are the adjustments to the dual-mode sorption model. (1 atm is equivalent to 1.013 bar)

In **Figure S11** graphs of the Langmuir adsorption parameters $C'_H \cdot b$ and the Henry solubility coefficient. K_D. *vs* critical temperature of the gas for the three membranes are compared[39]. From the calculated $C'_H \cdot b$ it can be concluded that the contribution from the Langmuir adsorption is more important than the contribution from Henry solubility in all the cases. As expected, the most condensable gas, CO_2, shows higher values for both parameters.

On the other hand. C'_H. is related to the frozen excess volume in the glass state. presented a more significant variation in its values than the other parameters. In general. it was observed that the membranes derived from the PIs that have methyl groups in the biphenyl unit presented C'_H values higher than their homologous that do not have such groups. This fact indicated that 6FDA-4MeBFAPB and 6FDA-6MeBFAPB membranes have more excess free volume, which agrees with the greatest FFV obtained for these materials (**Table S2**). Nevertheless. from the C'_H values. no significant differences could be established between them.

4. Conclusions

Three diamines bearing biphenyl units studied in this work were obtained with good yields and high purity. enough to be used as monomers in polycondensation reactions. The polyimides of high molecular weights were synthesized with these diamines and 6FDA by two-steps polycondensation reaction via chemical cyclization. All polymers exhibited good mechanical properties and were

readily soluble in common organic solvents. facilitating membrane formation. FT-IR and TGA results confirmed the complete imidization process and total solvent removal from the membranes. All PIs presented excellent thermal properties with a 10% weight loss above 450 °C and a char residue around 40% at 800 °C. It was demonstrated that introducing methyl groups in the biphenyl moiety reduces the internal rotation and produces polymers with high rigidity. This fact, combined with the presence of $(CF_3)_2$ group, causes a reduction in the chain packing. as can be seen from X-ray analysis. In addition. the polymer with methyl substituents (6FDA-4MeBFAPB and 6FDA-6MeBFAPB) has significantly higher FFV and, therefore. better gas permeability than 6FDA-BFAPB, the polymer without methyl substituents. Although some reduction in selectivity for methylated PIs was observed, it was not significant enough to prevent the improvement of the overall selectivity of these membranes and, thus, place the 6FDA-4MeBFAPB and 6FDA-6MeBFAPB membranes much closer to the Robeson limit than the 6FDA-BFAPB membrane. Interestingly, the number of methyl groups in the polymer chain was reflected in the FFV value. Thus, the PI with more methyl groups (6FDA-6MeBFAPB) had a higher FFV. However, this increase in FFV did not result in a further improvement of gas transport properties, as both 6FDA-4MeBFAPB and 6FDA-6MeBFAPB PIs exhibited very similar gas transport properties.

Finally. gas transport properties of the membranes were evaluated not only for pure gases but for real gas mixtures from pressures going from 3 to 25 bar.

Supporting Information

The Supporting Information is available free of charge via Internet at https://pubs.acs.org/

Acknowledgment

This work was financially supported by Mexico's PAPIIT AG100323 and CONAHCyT CF-2023-G-220 projects. Also, this work was supported by Spain's Agencia Estatal de Investigación (AEI) (Projects: PID2019-109403RB-C22 (AEI/FEDER, UE), PID2019-109403RB-C21 (AEI/FEDER, UE) and PID2020-118547GB-I00 (AEI/FEDER, UE) and by the Spanish Junta de Castilla y León (VA224P2). S.R-M. thanks Spain's Ministry of Science Innovation and Universities (MCIU) for a predoctoral FPU grant.

5. References

(1) Wang, X.-Y.; Hill, A. J.; Freeman, B. D.; Sanchez, I. C. Structural, Sorption and Transport Characteristics of an Ultrapermeable Polymer. *J. Memb. Sci.* **2008**, *314* (1–2), 15–23. https://doi.org/10.1016/j.memsci.2007.12.074.

(2) Han, Y.; Ho, W. S. W. Recent Advances in Polymeric Membranes for CO2 Capture. *Chinese J. Chem. Eng.* **2018**, *26* (11), 2238–2254. https://doi.org/10.1016/j.cjche.2018.07.010.

(3) Chuah, C. Y. Membranes for Gas Separation and Purification Processes. *Membranes (Basel).* **2022**, *12* (6), 622. https://doi.org/10.3390/membranes12060622.

(4) Ababneh, H.; AlNouss, A.; Karimi, I.; Al-Muhtaseb, S. Natural Gas Sweetening Using an Energy-Efficient, State-of-the-Art, Solid–Vapor Separation Process. *Energies* **2022**, *15* (14), 5286. https://doi.org/10.3390/en15145286.

(5) Kadirkhan, F.; Goh, P. S.; Ismail, A. F.; Wan Mustapa, W. N. F.; Halim, M. H. M.; Soh, W. K.; Yeo, S. Y. Recent Advances of Polymeric Membranes in Tackling Plasticization and Aging for Practical Industrial CO2/CH4 Applications—A Review. *Membranes (Basel).* **2022**, *12* (1), 71. https://doi.org/10.3390/membranes12010071.

(6) Robeson, L. M. The Upper Bound Revisited. *J. Memb. Sci.* **2008**, *320* (1–2), 390–400. https://doi.org/10.1016/j.memsci.2008.04.030.

(7) Qiu, W.; Xu, L.; Chen, C.-C.; Paul, D. R.; Koros, W. J. Gas Separation Performance of 6FDA-Based Polyimides with Different Chemical Structures. *Polymer (Guildf).* **2013**, *54* (22), 6226–6235. https://doi.org/10.1016/j.polymer.2013.09.007.

(8) Freeman, B. D. Basis of Permeability/Selectivity Tradeoff Relations in Polymeric Gas Separation Membranes. *Macromolecules* **1999**, *32* (2), 375–380. https://doi.org/10.1021/ma9814548.

(9) Yang, Z.; Guo, W.; Mahurin, S. M.; Wang, S.; Chen, H.; Cheng, L.; Jie, K.; Meyer, H. M.; Jiang, D.; Liu, G.; Jin, W.; Popovs, I.; Dai, S. Surpassing Robeson Upper Limit for CO2/N2 Separation with Fluorinated Carbon Molecular Sieve Membranes. *Chem* **2020**, *6* (3), 631–645. https://doi.org/10.1016/j.chempr.2019.12.006.

(10) Moon, J. D.; Freeman, B. D.; Hawker, C. J.; Segalman, R. A. Can Self-Assembly Address the Permeability/Selectivity Trade-Offs in Polymer Membranes? *Macromolecules* **2020**, *53* (14), 5649–5654. https://doi.org/10.1021/acs.macromol.0c01111.

(11) Plaza-Lozano, D.; Comesaña-Gándara, B.; de la Viuda, M.; Seong, J. G.; Palacio, L.; Prádanos, P.; de la Campa, J. G.; Cuadrado, P.; Lee, Y. M.; Hernández, A.; Alvarez, C.; Lozano, A. E. New Aromatic Polyamides and Polyimides Having an Adamantane Bulky Group. *Mater. Today Commun.* **2015**, *5*, 23–31. https://doi.org/10.1016/j.mtcomm.2015.10.001.

(12) Ma, X.-H.; Yang, S.-Y. Polyimide Gas Separation Membranes. In *Advanced Polyimide Materials*; Elsevier, 2018; pp 257–322. https://doi.org/10.1016/B978-0-12-812640-0.00006-8.

(13) Álvarez, C.; Lozano, Á. E.; Juan-y-Seva, M.; de la Campa, J. G. Gas Separation Properties of Aromatic Polyimides with Bulky Groups. Comparison of Experimental and Simulated Results. *J. Memb. Sci.* **2020**, *602*, 117959. https://doi.org/10.1016/j.memsci.2020.117959.

(14) de Abajo, J.; de la Campa, J. G.; Lozano, A. E. Designing Aromatic Polyamides and Polyimides for Gas Separation Membranes. *Macromol. Symp.* **2003**, *199* (1), 293–306. https://doi.org/10.1002/masy.200350925.

(15) Yampolskii, Y. P.; Belov, N. A.; Alentiev, A. Y. Fluorine in the Structure of Polymers: Influence on the Gas Separation Properties. *Russ. Chem. Rev.* **2019**, *88* (4), 387–405. https://doi.org/10.1070/RCR4861.

(16) Belov, N.; Chatterjee, R.; Nikiforov, R.; Ryzhikh, V.; Bisoi, S.; Kumar, A. G.; Banerjee, S.; Yampolskii, Y. New Poly(Ether Imide)s with Pendant Di-Tert-Butyl Groups: Synthesis, Characterization and Gas Transport Properties. *Sep. Purif. Technol.* **2019**, *217*, 183–194. https://doi.org/10.1016/j.seppur.2019.02.017.

(17) Dutta, R. C.; Bhatia, S. K. Atomistic Investigation of Mixed-Gas Separation in a Fluorinated Polyimide Membrane. *ACS Appl. Polym. Mater.* **2019**, *1* (6), 1359–1371. https://doi.org/10.1021/acsapm.9b00146.

(18) Abdulhamid, M. A.; Genduso, G.; Ma, X.; Pinnau, I. Synthesis and Characterization of 6FDA/3,5-Diamino-2,4,6-Trimethylbenzenesulfonic Acid-Derived Polyimide for Gas Separation Applications. *Sep. Purif. Technol.* **2021**, *257*, 117910. https://doi.org/10.1016/j.seppur.2020.117910.

(19) Xu, Z.; Croft, Z. L.; Guo, D.; Cao, K.; Liu, G. Recent Development of Polyimides: Synthesis, Processing, and Application in Gas Separation. *J. Polym. Sci.* **2021**, *59* (11), 943–962. https://doi.org/10.1002/pol.20210001.

(20) Al-Masri, M.; Kricheldorf, H. R.; Fritsch, D. New Polyimides for Gas Separation. 1. Polyimides Derived from Substituted Terphenylenes and 4,4‘-(Hexafluoroisopropylidene)Diphthalic Anhydride. *Macromolecules* **1999**, *32* (23), 7853–7858. https://doi.org/10.1021/ma9910742.

(21) Wang, J.; Li, N.; Zhang, F.; Zhang, S.; Liu, J. Synthesis and Properties of Soluble Poly[Bis(Benzimidazobenzisoquinolinones)] Based on Novel Aromatic Tetraamine Monomers. *Polymer (Guildf).* **2009**, *50* (3), 810–816. https://doi.org/10.1016/j.polymer.2008.12.007.

(22) Dhara, M. G.; Banerjee, S. Fluorinated High-Performance Polymers: Poly(Arylene Ether)s and Aromatic Polyimides Containing Trifluoromethyl Groups. *Prog. Polym. Sci.* **2010**, *35* (8), 1022–1077. https://doi.org/10.1016/j.progpolymsci.2010.04.003.

(23) Sen, S. K.; Dasgupta, B.; Banerjee, S. Effect of Introduction of Heterocyclic Moieties into Polymer Backbone on Gas Transport Properties of Fluorinated Poly(Ether Imide) Membranes. *J. Memb. Sci.* **2009**, *343* (1–2), 97–103. https://doi.org/10.1016/j.memsci.2009.07.014.

(24) White, L. S.; Blinka, T. A.; Kloczewski, H. A.; Wang, I. Properties of a Polyimide Gas Separation Membrane in Natural Gas Streams. *J. Memb. Sci.* **1995**, *103* (1–2), 73–82. https://doi.org/10.1016/0376-7388(94)00313-N.

(25) Zhuo, L.; Kou, K.; Wang, Y.; Yao, P.; Wu, G. Synthesis of Soluble and Thermally Stable Polyimides with Phthalimide as Pendent Group from Pyridine-Containing Triamine. *J. Mater. Sci.* **2014**, *49* (14), 5141–5150. https://doi.org/10.1007/s10853-014-8222-3.

(26) Yang, C. P.; Hsiao, S. H.; Chen, K. H. Organosoluble and Optically Transparent Fluorine-Containing Polyimides Based on 4,4′-Bis(4-Amino-2-Trifluoromethylphenoxy)-3,3′,5,5′ -

Tetramethylbiphenyl. *Polymer (Guildf).* **2002**, *43* (19), 5095–5104. https://doi.org/10.1016/S0032-3861(02)00359-2.

(27) Koros, W. J.; Paul, D. R. Design Considerations for Measurement of Gas Sorption in Polymers by Pressure Decay. *J. Polym. Sci. Polym. Phys. Ed.* **1976**, *14* (10), 1903–1907. https://doi.org/10.1002/pol.1976.180141014.

(28) Yang, C.-P.; Hsiao, S.-H.; Hsu, M.-F. Organosoluble and Light-Colored Fluorinated Polyimides from 4,4?-Bis(4-Amino-2-Trifluoromethylphenoxy)Biphenyl and Aromatic Dianhydrides. *J. Polym. Sci. Part A Polym. Chem.* **2002**, *40* (4), 524–534. https://doi.org/10.1002/pola.10113.

(29) Klopman, G. Chemical Reactivity and the Concept of Charge- and Frontier-Controlled Reactions. *J. Am. Chem. Soc.* **1968**, *90* (2), 223–234. https://doi.org/10.1021/ja01004a002.

(30) Lozano, A. E.; de Abajo, J.; de la Campa, J. G. Quantum Semiempirical Study on the Reactivity of Silylated Diamines in the Synthesis of Aromatic Polyamides. *Macromol. Theory Simulations* **1998**, *7* (1), 41–48. https://doi.org/10.1002/(SICI)1521-3919(19980101)7:1<41::AID-MATS41>3.0.CO;2-G.

(31) Sánchez-Márquez, J. Reactivity Indices for Natural Bond Orbitals: A New Methodology. *J. Mol. Model.* **2015**, *21* (4), 82. https://doi.org/10.1007/s00894-015-2610-8.

(32) RECIO, R.; PALACIO, L.; PRADANOS, P.; HERNANDEZ, A.; LOZANO, A.; MARCOS, A.; DELACAMPA, J.; DEABAJO, J. Gas Separation of 6FDA–6FpDA MembranesEffect of the Solvent on Polymer Surfaces and Permselectivity. *J. Memb. Sci.* **2007**, *293* (1–2), 22–28. https://doi.org/10.1016/j.memsci.2007.01.022.

(33) Cecopieri-Gómez, M. L.; Palacios-Alquisira, J.; Domínguez, J. M. On the Limits of Gas Separation in CO2/CH4, N2/CH4 and CO2/N2 Binary Mixtures Using Polyimide Membranes. *J. Memb. Sci.* **2007**. https://doi.org/10.1016/j.memsci.2007.01.034.

(34) Raymond, P. C.; Koros, W. J.; Paul, D. R. Comparison of Mixed and Pure Gas Permeation Characteristics for CO2 and CH4 in Copolymers and Blends Containing Methyl Methacrylate Units. *J. Memb. Sci.* **1993**, *77* (1), 49–57. https://doi.org/10.1016/0376-7388(93)85234-N.

(35) Kim, T. H.; Koros, W. J.; Husk, G. R.; O'Brien, K. C. Relationship between Gas Separation Properties and Chemical Structure in a Series of Aromatic Polyimides. *J. Memb. Sci.* **1988**, *37* (1), 45–62. https://doi.org/10.1016/S0376-7388(00)85068-1.

(36) Wang, Y. C.; Huang, S. H.; Hu, C. C.; Li, C. L.; Lee, K. R.; Liaw, D. J.; Lai, J. Y. Sorption and Transport Properties of Gases in Aromatic Polyimide Membranes. *J. Memb. Sci.* **2005**, *248* (1–2), 15–25. https://doi.org/10.1016/j.memsci.2004.09.015.

(37) Neyertz, S.; Brown, D.; Pandiyan, S.; van der Vegt, N. F. A. Carbon Dioxide Diffusion and Plasticization in Fluorinated Polyimides. *Macromolecules* **2010**, *43* (18), 7813–7827. https://doi.org/10.1021/ma1010205.

(38) Qiu, W.; Chen, C.-C.; Xu, L.; Cui, L.; Paul, D. R.; Koros, W. J. Sub- T g Cross-Linking of a Polyimide Membrane for Enhanced CO 2 Plasticization Resistance for Natural Gas Separation. *Macromolecules* **2011**, *44* (15), 6046–6056. https://doi.org/10.1021/ma201033j.

(39) Erb, A. J.; Paul, D. R. Gas Sorption and Transport in Polysulfone. *J. Memb. Sci.* **1981**, *8* (1), 11–22. https://doi.org/10.1016/S0376-7388(00)82135-3.

For Table of Contents Only